Available online at www.sciencedirect.com
ScienceDirect
Scripta Materialia 64 (2011) 605–608
Scripta MATERIALIA
www.elsevier.com/locate/scriptamat

A universal scaling of planar fault energy barriers in face-centered cubic metals

Z.H. Jin,[a,b,*] S.T. Dunham,[c] H. Gleiter,[b] H. Hahn[b] and P. Gumbsch[d,e]

[a]*School of Materials Science and Engineering, Shanghai Jiao Tong University, 200240 Shanghai, People's Republic of China*
[b]*Institut für Nanotechnologie (INT), Karlsruher Institut für Technologie, 76021 Karlsruhe, Germany*
[c]*Department of Electrical Engineering, University of Washington, Seattle, WA 98195, USA*
[d]*Institut für Zuverlässigkeit von Bauteilen und Systemen (IZBS), Karlsruher Institut für Technologie, 76131 Karlsruhe, Germany*
[e]*Fraunhofer Institut für Werkstoffmechanik (IWM), 79108 Freiburg, Germany*

Received 7 September 2010; revised 16 November 2010; accepted 18 November 2010
Available online 23 November 2010

Minimum energy paths for generating intrinsic, extrinsic and twin planar faults were calculated for a number of face-centered cubic (fcc) metals via ab initio techniques. It is found that when the lattice is faulted sequentially, the interaction with the existing fault tends to remain minimal for nearly all the fcc metals. Accordingly, a universal scaling law may be deduced based on a single parameter, namely the ratio between the intrinsic stacking fault energy and the relevant energy barrier.

Keywords: Metal and alloys; Generalized stacking fault energies; Lattice dislocation and planar fault; Twinning; First-principles calculation

The plastic deformation of crystalline ductile materials at low temperatures is mediated by dislocation slip as well as by mechanical twinning [1–3]. In comparison to coarse-grained polycrystalline materials, an enhanced dislocation density due to emission of partial dislocations, perfect dislocations and microtwins from grain boundary sources have been reported in several nanostructured face-centered cubic (fcc) metals [4–9]. The underlying fundamental processes and defect structures are not yet fully understood. For example, in materials with high energies of intrinsic stacking faults (ISFs) and high coherent twin boundary energies such as Al, twinning is believed to be difficult. Nevertheless, atomistic simulations and experimental observations suggest twinning occurs readily in Al [4,5]. On the other hand, recent experiments indicate that yield strength as well as ductility can be enhanced in materials with low ISF energies such as Cu [10–13] and stainless steels [14] due to preexisting nanoscale twins. However, similar effects do not seem to exist in Al [15–19].

Energies of planar faults are fundamental properties underlying mechanical deformation, solid-state phase transformation and diffusion of alloying elements in materials of different crystalline structures [1–3]. The minimum energy barrier, namely the unstable fault energy, provides an essential measure to produce a stable fault within a perfect lattice [20–22]. Both stable and unstable fault energies can be calculated according to the minimum energy pathway along a fault plane, also known as the generalized stacking-fault (GSF) energy curve or γ-surfaces. Although GSF energies for fcc metals and alloys have been well-studied recently via various computational approaches [23–34], it remains unclear how planar faults multiply and interact with existing faults in different materials.

In this paper, energies associated with ISFs extrinsic stacking faults (ESFs) and twin faults (TFs) in fcc lattice are calculated to elucidate correlations among stable and unstable fault energies. To clarify the general material dependence, we shall try to deduce a universal scaling law based on a single parameter, A, the ratio between the ISF energy and the unstable stacking fault energy associated with an ISF. In order to do so, the minimum energy barriers of following paths were calculated (see Fig. 1 for Al, Cu and Pt):

- γ(perfect lattice → ISF): the energy path of a crystal when it is transformed from a perfect fcc lattice into an ISF of energy γ_{isf}. The saddlepoint of the transition defines the unstable stacking fault energy, γ_{usf} (Fig. 1, left-hand diagram).

* Corresponding author at: School of Materials Science and Engineering, Shanghai Jiao Tong University, 200240 Shanghai, People's Republic of China. Tel./fax: +86 21 54745427; e-mail: jinzh@sjtu.edu.cn

1359-6462/$ - see front matter © 2010 Acta Materialia Inc. Published by Elsevier Ltd. All rights reserved.
doi:10.1016/j.scriptamat.2010.11.033

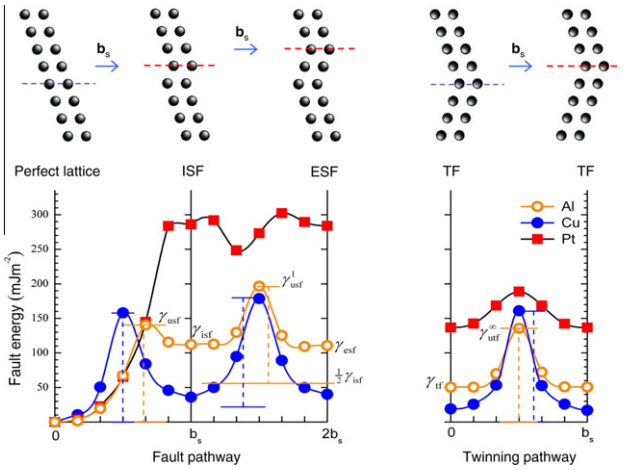

Figure 1. Fault/twinning pathways produced by displacing the two parts of a crystal along a (1 1 1) fault plane. The displacement along each pathway is given by the Burgers vector of a Shockley partial dislocation, $\mathbf{b}_s = \frac{a_0}{6}\langle 1\,1\,\bar{2}\rangle$. Upper panel: schematic of stacking fault formation via $\{1\,1\,1\}\,\langle 1\,1\,\bar{2}\rangle$ slip in fcc metals. Lower panel: minimum-energy pathways (γ-surfaces) for Al, Cu and Pt, obtained via converged NEB-DFT calculations. Along each path, five images were used to build the elastic band between the given initial and final state. The saddlepoint energy (the energy extremes) defines the unstable fault energy. The γ-surface is defined by $\gamma = (E - E_0)/A$, where E is the energy of the optimized elastic band, E_0 is the energy of the fault-free state and A is the area of the fault plane. Stable and unstable energies are marked following the pathway for Al. Vertical bars measure the relation $\gamma_{usf} \simeq \gamma^1_{utf} - \frac{1}{2}\gamma_{isf} \simeq \gamma^\infty_{utf}$, which applies to Al and Cu but not for Pt.

- γ(ISF → ESF): the energy path of a crystal when it transforms from an ISF into an ESF of energy γ_{esf}. The saddlepoint of the transition defines the unstable energy, γ^1_{utf} (Fig. 1, middle diagram).
- γ(TF → TF′): the energy path for twinning based on a single twin boundary or a TF of energy γ_{tf}. The saddlepoint energy defines the unstable energy for twinning, γ^∞_{utf} (Fig. 1, right-hand diagram). In this way an extrinsic fault may develop into two well-separated twin faults to form a thick twin lamella.

We consider all the common fcc metals in our calculations (cf. Table 1). The γ-surfaces were mapped out via fully converged calculations with the climbing-image nudged elastic band (ciNEB) method [35] in combination with the ab initio density-functional theory (DFT). The NEB method [36] is an efficient technique for finding corresponding minimum energy paths between a given initial state and a final state of a transition, with essentially no limitation on the degrees of freedom for atomic/ionic relaxations. DFT computations were performed using the Vienna ab initio simulation package (VASP) [37,38]. The full-potential projector augmented-wave method was used with core–valence electron interactions treated within the standard Blöchl scheme [39,40]. Details of computations can be found in Supplementary data.

Converged minimum-energy pathways are shown in Figure 1 (lower panel) for Al, Cu and Pt. All obtained stable and unstable fault energies are summarized in Table 1. As may be seen in Table 1, these fault energies were found to correlate according to the following linear relations:

(i) For stable faults, the energy γ_{esf} is close to γ_{isf} and nearly twice γ_{tf}, i.e. $\gamma_{isf} \simeq \gamma_{esf} \simeq 2\gamma_{tf}$, consistent with the well-known rule of thumb reported in the literature [1]. This implies that both ISFs and ESFs can be thought of as one pair of TFs on neighboring planes, with energies nearly the same as for two well-separated TFs.

(ii) When a fault is produced by sliding two parts of a crystal across a single atomic plane, the transition state energy satisfies

$$\gamma_{usf} \simeq \gamma^1_{utf} - \frac{1}{2}\gamma_{isf} \simeq \gamma^\infty_{utf} \tag{1}$$

This relation implies that the resisting force of the lattice neither changes significantly from one pathway to another, nor is altered by an existing fault. In other words, when the lattice is faulted sequentially, Eq. (1) holds as long as the interaction with existing fault remains minimal. It applies for nearly all metals we considered so far except for Pt, which shows reduced energy barriers along both ESF and TF pathways (Fig. 1).

Based on these observations, the ratio $\Lambda \equiv \gamma_{isf}/\gamma_{usf}$ (see Table 1) can be used as a characteristic material measure by which a scaling law can be deduced according to Eq. (1):

$$\gamma^1_{utf}/\gamma_{usf} \simeq \Lambda/2 + 1 \tag{2}$$

As can be seen in Figure 2a, the plot reveals that, from Ag to Pb, our data scales remarkably well according to the linear relation, Eq. (2). The Lennard–Jones (LJ) system has been included as a limiting case on the left-hand side because for this well-studied model material the stacking fault and TF energies are nearly zero, with $\Lambda \simeq 0$ and $\gamma^1_{utf}/\gamma_{usf} \simeq 1$. On the right-hand side,

Table 1. Stable and unstable fault energies calculated using ciNEB-DFT methods (units in mJ m^{-2}). Correlation parameters, α_0, α_1, β_1 and β_∞, are dimensionless ratios defined according to $\gamma_{isf} = \alpha_0\gamma_{tf}$, $\gamma_{esf} = \alpha_1\gamma_{tf}$, $\gamma^1_{utf} - \frac{1}{2}\gamma_{isf} = \beta_1\gamma_{usf}$ and $\gamma^\infty_{utf} = \beta_\infty\gamma_{usf}$, respectively. The parameters α_0, α_1 are close to 2, and β_1 and β_∞ are close to unity for all metals considered except for Pt. The ratio $\Lambda \equiv \gamma_{isf}/\gamma_{usf}$ has been introduced as a characteristic material measure.

	γ_{isf}	γ_{esf}	γ_{tf}	γ_{usf}	γ^1_{utf}	γ^∞_{utf}	α_0	α_1	β_1	β_∞	Λ
Silver	16	12	8	91	100	93	2.08	1.56	**1.0**	1.01	**0.18**
Copper	36	40	18	158	179	161	2.0	2.22	**1.02**	1.02	**0.23**
Gold	25	27	12	68	79	72	1.98	2.16	**0.98**	1.04	**0.36**
Nickel	133	138	65	258	323	251	2.05	2.12	**0.99**	0.97	**0.52**
Iridium	334	327	160	625	818	624	2.09	2.04	**1.04**	1.0	**0.53**
Palladium	134	129	63	202	261	190	2.13	2.05	**0.96**	0.94	**0.66**
Aluminum	112	112	50	140	196	135	2.24	2.24	**1.0**	0.96	**0.80**
Lead	48	48	23	55	79	53	2.07	2.05	**1.0**	0.96	**0.88**
Platinum	286	284	137	286	305	189	2.09	2.07	**0.57**	0.66	**1.0**

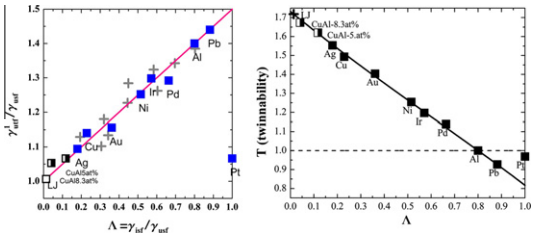

Figure 2. (a, left) Scaling plot of stable and unstable fault energies. Filled symbols represent our ciNEB-DFT results. Cross symbols in grey are data obtained via NRLTB methods (non-NEB calculations) [26,27]. With increasing Λ, those elements are Ag, Pb, Cu, Pd, Au, Ir, Pb′, Al, Pt, Ir′ (a prime appears if a different set of tight-binding parameters was used for the same element). For Cu–Al alloys (at.% Al), data were taken from Ref. [32]. (b, right) The universal trend of twinning according to a twinnability measure (T) defined in Ref. [45].

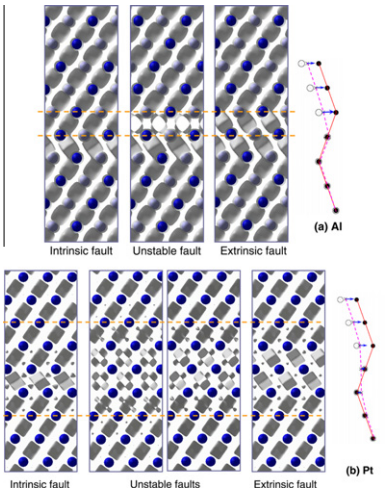

Figure 3. Charge distributions associated with forming an ESF in Al (a) and Pt (b). Vector plots at the right-hand side represent ionic displacements between the saddlepoint image and its neighboring "uphill" image (cross symbols, cf. Fig. 1, lower panel), magnified by a factor of 2.5 (ionic positions of the initial image (ISF) and the final image (ESF) are drawn with open circles and dots, respectively; as visual guides, dashed and full lines are used to indicate ionic positions at different states). Charges are depicted at an isosurface value, 0.18 $e\text{Å}^{-3}$ for Al and 0.23 $e\text{Å}^{-3}$ for Pt, with ions shown by blue balls. In both metals the atomic bonds are highly directional. Like other metals, redistribution of charges in Al appears almost solely within the two adjacent fault planes, emphasizing that the interaction between faults tends to be minimal. In Pt, extended redistributions across about 5 (1 1 1) layers (marked by horizontal dashed lines) are observed, suggesting strong coupling between faults or change of bonds involving multiple (1 1 1) layers for both stable and unstable fault configurations.

Al ($\Lambda \simeq 0.8$) and Pb ($\Lambda \simeq 0.88$) are found to be quite close to the other limiting case, a fcc material with $\Lambda = 1$ and $\gamma^1_{utf}/\gamma_{usf} = 3/2$. For Pt the value of Λ is found to be exactly unity; however, the $\gamma^1_{utf}/\gamma_{usf}$ ratio for Pt turns out to be merely 1.07, far from expected. To understand why Eq. (1) applies to other metals but not to Pt, we examined both ionic displacements and charge distributions when the lattice is faulted.

For metals with large Λ values, charge density plots reveal that γ-surfaces are dominated by directional bonds associated with the s–p band for the simple metals such as for Al and Pb or with a partially filled d-band for transition metals such as Ni, Pd, Ir and Pt. When two parts of a crystal are displaced relative to each other, the bonds retreat locally to resist shear (see e.g. Fig. 3a for Al). The reduced bonding gives rise to the energy of the γ-surface. If the change in bonding characteristic is confined within two adjacent planes, the energy barrier remains unaltered from one path to another (Eq. (1) and Fig. 1). This justifies that γ_{usf}, together with γ_{isf}, may define a characteristic material measure (Λ) such that Eq. (2a) applies.

As shown in Figure 3a, to generate a fault in Al, only ions belonging to the two adjacent {1 1 1} fault planes undergo large strains and significant charge redistributions. That is, as a fault (e.g. ESF or TF) is generated based on an existing fault (e.g. ISF) a minimum interaction with the existing fault is maintained due to the lattice rigidity (see Fig. 2a).

This does not apply for Pt. In the case of Pt, the electronic structure is changed significantly in at least two {1 1 1} atomic planes. Several atomic planes are therefore involved and couple strongly as a new fault is generated (Fig. 3b). As can be seen in Figure 3b, together with the change in bonding characteristic, atoms in several adjacent {1 1 1} lattice planes are displaced due to strong interactions between the existing fault and the newly generated fault.

The linear scaling shown in Figure 2a is also supported by results in several previous publications [25–32]. Data obtained recently for a number of fcc elements via the Naval Research Lab Tight-Binding (NRLTB) codes [26,27] have been depicted in the same plot. They scale equally well and obey the same trend despite the fact that the calculated Λs for the same element depend on the particular set of tight-binding parameters. While stacking fault energies of alloy systems may depend strongly on alloying elements and concentrations, we found that Eq. (2) still applies for Cu–Al alloys [32] (Fig. 2a).

For metals of low-Λ, such as Cu with a filled d-band, the bonding can be mapped quite well for central-force type atomic interactions. The scaling law revealed by Eq. (2) in general applies. In some cases, central-force interatomic potentials underestimate the ratio $\gamma^1_{utf}/\gamma_{usf}$ although the ratio Λ may be reproduced reasonably well [26,28]. The scaling law (Eq. (2)) therefore constitutes a useful guide for fitting empirical interatomic interactions (Supplementary data and [41]).

A more generalized version of Eq. (2) can be written as $\gamma^1_{utf}/\gamma_{usf} \simeq \Lambda/2 + \beta_1$. The minimum interaction principle satisfies if $\beta_1 \simeq 1$ (see Table 1) and the planar fault configuration in this case is characterized by localized bonding effects. Note that for hcp metals such as Mg, the same scaling rule ($\beta_1 \simeq 1$) is obeyed when faults are generated sequentially along basal planes [42].

In nanostructured fcc metals, the trend to emit partial dislocations, perfect dislocations and twins can be understood in terms of the energy barriers on γ-surfaces. For large values of Λ (e.g. Al), emission of trailing partials leading to perfect dislocations is generally favored over twin nucleation ($\gamma_{usf} - \gamma_{isf}$ vs. $\gamma^1_{utf} - \gamma_{isf}$), but once nucleated, twins can grow readily ($\gamma^{\infty}_{utf} - \gamma_{tf}$ vs. γ_{usf}) [4,15–18]. For small values of Λ (e.g. Cu), there is little difference in the barriers associated with twin growth and the emission of independent leading partials, so the latter is likely to dominate the response to deformation and

the strengthening role due to existing twins can be expected to be most significant [10–16].

The scaling law of Eq. (2) encompasses a broad range of fcc materials. If Eq. (2) holds, it can be readily applied to reveal a general trend of mechanical twinning for fcc metals. Based on mechanical analyses of dislocation vs. twin emission from a crack-tip [43], a dimensionless measure, the so-called "twinnability", was introduced by Tadmor and Hai [44] as an intrinsic material property. Asaro and Suresh [45] proposed that in nanostructured fcc materials, the relative occurrence of dislocation vs. microtwin emission from grain boundary sources is similar to that from a crack-tip. They considered the most favorable geometry condition for twinning and derived a modified twinnability measure [45]:

$$T = \sqrt{(3\gamma_{usf} - 2\gamma_{isf})/\gamma^{1}_{utf}} \tag{3}$$

The twinnability, T, offers a mechanical criterion: if $T > 1$, twin emission is favored over the emission of a trailing partial dislocation and thus of the emission of a perfect dislocation. Using the single ratio Λ and our scaling law, T can be converted into:

$$T \simeq \sqrt{(3 - 2\Lambda)/(1 + \Lambda/2)} \tag{4}$$

Using the same set of data as in Figure 2a, the computed twinnability T according to Eq. (3) is plotted together with the scaling trend based on Eq. (4) as shown in the right diagram of Figure 2. It is evident that to evaluate the trend of twin emission for different fcc materials, one has to consider Λ instead of the ISF energy alone.

Eq. (4) suggests that in general twinning should be prohibited in nanostructured metals with $\Lambda > 0.8$. Otherwise, twinning constitutes a competitive mode of deformation along with dislocation-mediated slip. This is in agreement with experimental observations of twinning in metals such as Cu, Ni and Pd [7–9]. In the plot, Al represents a marginal case for the occurrence of twin emission, which is also consistent with the experimental conclusion that twinning rarely occurs for this metal [18]. However, it has been argued that in the nanoscale domain, small grain size increases the partial dislocation separation distance, aiding twinning [7]. For Pt, twin emission is most difficult according to our results as well as NRLTB calculations [26,27]. Since the twinnability measure given by Eqs. (3) and (4) relies on the assumption that microtwin emission from grain boundary sources is similar to that from a crack-tip, it may fail if deformation twinning occurs via different mechanisms [46–50].

We thank M. Hettler for technical support on parallel computations. S.T.D. acknowledges support from Forschungszentrum Karlsruhe and the Center for Functional Nanostructures, KIT. This work was funded by the Deutsche Forschungsgemeinschaft (DFG) and the National Natural Science Foundation of China (Grant Nos. 50890174 and 50971088).

Supplementary data associated with this article can be found, in the online version, at doi:10.1016/j.scriptamat.2010.11.033.

[1] J.P. Hirth, J. Lothe, Theory of Dislocations, Wiley, New York, 1982.
[2] J.A. Venables, Philos. Mag. 6 (1961) 379.
[3] J.W. Christian, S. Mahajan, Prog. Mater. Sci. 39 (1995) 1.
[4] V. Yamakov et al., Nat. Mater. 1 (2002) 45.
[5] M.W. Chen et al., Science 300 (2003) 1275.
[6] J. Schiøtz, K.W. Jacobsen, Science 301 (2003) 1357.
[7] X.Z. Liao et al., Appl. Phys. Lett. 84 (2004) 592.
[8] H. Rösner, J. Markmann, J. Weissmüller, Philos. Mag. Lett. 84 (2004) 321.
[9] X. Wu, Y.T. Zhu, M.W. Chen, E. Ma, Scripta Mater. 54 (2006) 1685.
[10] Y.F. Shen et al., Scripta Mater. 52 (2005) 989.
[11] L. Lu et al., Science 304 (2004) 422.
[12] L. Lu, X. Chen, X. Huang, K. Lu, Science 323 (2009) 607.
[13] L. Lu et al., Acta Mater. 53 (2005) 21169.
[14] X. Zhang et al., Appl. Phys. Lett. 84 (2004) 1096.
[15] Z.H. Jin et al., Scripta Mater. 54 (2006) 1163.
[16] Z.H. Jin et al., Acta Mater. 56 (2008) 1126.
[17] A. Frøseth, H.V. Swygenhoven, P.M. Derlet, Acta Mater. 52 (2004) 2259.
[18] M.A. Meyers, A. Mishra, D.J. Benson, Prog. Mater. Sci. 51 (2006) 427.
[19] T. Zhu, J. Li, Prog. Mater. Sci. 55 (2010) 710.
[20] V. Vitek, Philos. Mag. 18 (1968) 773.
[21] A.T. Paxton, P. Gumbsch, M.A. Methfessel, Philos. Mag. Lett. 63 (1991) 267.
[22] D. Roundy, C.R. Krenn, M.L. Cohen, J.W. Morris Jr., Phys. Rev. Lett. 82 (1999) 2713.
[23] J.A. Zimmerman, H. Gao, F.F. Abraham, Model. Simul. Mater. Sci. 8 (2000) 103.
[24] G. Lu et al., Phys. Rev. B 65 (2002) 064102.
[25] S. Ogata, J. Li, S. Yip, Science 298 (2002) 807.
[26] E.B. Tadmor, N. Bernstein, J. Mech. Phys. Solids 52 (2004) 2507.
[27] N. Bernstein, E.B. Tadmor, Phys. Rev. B 69 (2004) 094116.
[28] H.V. Swygenhoven, P.M. Derlet, A.G. Frøseth, Nat. Mater. 3 (2004) 399.
[29] S. Ogata, J. Li, S. Yip, Phys. Rev. B 71 (2005) 224102.
[30] D.J. Siegel, Appl. Phys. Lett. 87 (2005) 121901.
[31] D. Finkenstadt, D.D. Johnson, Phys. Rev. B 73 (2006) 024101.
[32] S. Kibey, J.B. Liu, D.D. Johnson, H. Sehitoglu, Appl. Phys. Lett. 89 (2006) 191911.
[33] M. Jahnátek, J. Hafner, M. Krajčí, Phys. Rev. B 79 (2009) 224103.
[34] Y. Wang, J. Li, Acta Mater. 58 (2010) 1212.
[35] G. Henkelman, B.P. Uberuaga, H. Jónsson, J. Chem. Phys. 113 (2000) 9901.
[36] H. Jónsson, G. Mills, K.W. Jacobsen, Nudged elastic band method for finding minimum energy paths of transitions, in: B.J. Berne, C. Ciccotti, D.F. Coker (Eds.), Classical and Quantum Dynamics in Condensed Phase Simulations, World Scientific, Singapore, 1998, pp. 385–404.
[37] G. Kresse, J. Hafner, Phys. Rev. B 47 (1993) 558.
[38] G. Kresse, J. Furthmüller, Phys. Rev. B 54 (1996) 11169.
[39] P.E. Blöchl, Phys. Rev. B 50 (1994) 17953.
[40] G. Kresse, D. Joubert, Phys. Rev. B 59 (1999) 1758.
[41] Y. Mishin, M. Asta, J. Li, Acta Mater. 58 (2010) 1117.
[42] J. Han, X.M. Su, Z.H. Jin, Y.T. Zhu, Scripta Mater. (2010), doi:10.1016/j.scriptamat.2010.11.034.
[43] J.R. Rice, J. Mech. Phys. Solids 40 (1992) 239.
[44] E.B. Tadmor, S.A. Hai, J. Mech. Phys. Solids 51 (2003) 765.
[45] R.J. Asaro, S. Suresh, Acta Mater. 53 (2005) 3369.
[46] V.R. Parameswaran, J. Weertman, J. Mater. Sci. 4 (1969) 646.
[47] E. El-Danaf, S.R. Kalidindi, R.D. Doherty, Metall. Mater. Trans. A30 (1999) 1223.
[48] D.H. Warner, W.A. Curtin, S. Qu, Nat. Mater. 6 (2007) 876.
[49] Y.B. Wang, M.L. Sui, Mater. Sci. Forum 63 (2010) 633.
[50] Q. Yu et al., Nature 463 (2010) 335.